RSC Advances



This is an *Accepted Manuscript*, which has been through the Royal Society of Chemistry peer review process and has been accepted for publication.

Accepted Manuscripts are published online shortly after acceptance, before technical editing, formatting and proof reading. Using this free service, authors can make their results available to the community, in citable form, before we publish the edited article. This Accepted Manuscript will be replaced by the edited, formatted and paginated article as soon as this is available.

You can find more information about *Accepted Manuscripts* in the **Information for Authors**.

Please note that technical editing may introduce minor changes to the text and/or graphics, which may alter content. The journal's standard <u>Terms & Conditions</u> and the <u>Ethical guidelines</u> still apply. In no event shall the Royal Society of Chemistry be held responsible for any errors or omissions in this *Accepted Manuscript* or any consequences arising from the use of any information it contains.



Cite this: DOI: 10.1039/c0xx00000x

www.rsc.org/xxxxxx

ARTICLE TYPE

Reduction of 4-nitrophenol to 4-aminopenol using novel $Pd@Ni_xB - SiO_2/RGO$ nanocomposite: Enhanced hydrogen spillover and high catalytic performance

Rahul Krishna^a, Diana M. Fernandes^b, Valdemar F. Domingos^c, Edivagner S. Ribeiro^d, João Campos Gil^d, Catarina Dias^e, Joao Ventura^e, Cristina Freire^b, Elby Titus^{a,*}

Received (in XXX, XXX) Xth XXXXXXXXX 20XX, Accepted Xth XXXXXXXX 20XX DOI: 10.1039/b000000x

Nanocomposite catalyst containing palladium-nickel boride-silica and reduced graphene oxide (Pd@Ni_xB-SiO₂/RGO, abbreviated as Pd@NSG) was successfully fabricated and discussed its enhanced hydrogen spillover mechanism and high catalytic performance towards reduction of 4-nitrophenol (4-NP) to 4-aminophenol (4-AP). The structure, composition and morphology of Pd@NSG nanocomposite were characterized by various techniques. The H₂ adsorption experiment directly reveals the spillover effect on Pd@NSG nanocomposite and enhanced H₂ uptake capacity (0.7 wt. %) compared to SiO₂/RGO (0.05 wt. %) under 50 bar pressure at RT. 4-NP reduction reaction shows remarkably high activity (120 s) of Pd@NSG compared to Ni_xB-SiO₂/RGO (7200 s) with excellent stability up to 5 cycles. Both the experiments showed, the facile H₂ dissociation on Pd (active sites) activator and subsequent transportation of hydrogen atom on receptor sites (Ni_xB-SiO₂/RGO and 4-NP, respectively).

Introduction

Noble metals (Pd, Ag, Au and Pt) nanoparticles based reduced graphene oxide (RGO) composites have recently gained a lot of interest due to their high catalytic activity and chemical inertness. However, high costs and limited number of noble metal resources urge a restricted consumption of expensive materials with the retention of catalytic property for progressive 25 research and real field of interest. A combination of other less expensive materials may be a better solution to deal with this issue. Raw transition metal elements, especially Fe, Co and Ni are best suited propositions owing to their low cost, wide availability and co-catalytic activity. A very recent work shows the methanol electro-oxidation using Fe₃O₄@Au/RGO nanocomposite with high performance.

Attractive results were also obtained by the Wu et al. for methylene blue (MB) dye reduction using the Pt-Fe₃O₄/RGO nanocomposite. ¹² Qin *et al.* also successfully demonstrated the recyclable catalytic performance of the PdNi@Pd/RGO 50 nanocomposite for hydrogen generation via formic acid decomposition. 13 On the other hand, 4-nitrophenol (4-NP) is a pollutant and an effluent in many chemicals and drug industries and therefore its efficient quick degradation is required.14 Nevertheless,, its reduction is only possible in the presence of a 55 catalyst. 15 For this hydrogenation process, several kinds of catalysts are still being investigated and several examples can be found in the scientific literature. 14,16-19 A recent work demonstrated the successful reduction of 4-NP using Pd/RGO nanocomposite in a very short time (120 sec).²⁰ Ji et al. also reported the reduction of 4-NP by Ni/RGO.²¹ Although, the reduction process of 4-NP with Ni/RGO was too slow compared to Pd/RGO. The fast reduction in Pd was evident due to the high spillover capability and its noble behaviour. 13,20,22 Considering the high cost of Pd and slow reduction process using Ni/RGO, it 65 is crucial to develop new materials for this catalysis reaction with retention of catalytic activity and low price.

The synthesis of finely divided Ni (without surfactant) is critical due to its magnetic behaviour (agglomeration of nanoparticles) and the requirement of harsh reaction conditions. ²³
⁷⁰ For example, to synthesise the Ni nanoparticles, the occasional involvement of toxic chemicals (hydrazine hydrate) and high-temperature reaction conditions (to decompose the organometallic precursors) disfavour the process easiness. ²⁴⁻²⁷ Furthermore, Ni_xB can be easily synthesised by the simple ⁷⁵ reduction of Ni²⁺ ions by sodium borohydride (NaBH₄). ²⁸ Ni_xB is

^a Centre for Mechanical Technology and Automation (TEMA),
Department of Mechanical Engineering, University of Aveiro, 3810-193,
Portugal. Tel: +351-234370830; Fax: +351-234370953

^{35 *}Email: elby@ua.pt

 ^b REQUIMTE/LAQV, Department of Chemistry and Biochemistry, Faculty of Sciences, University of Porto, 4169-007 Porto, Portugal
 ^cLIP-Coimbra, University of Coimbra, Coimbra 3004-516, Portugal
 ^d CFisUC, Department of Physics, University of Coimbra, Coimbra 3004-516, Portugal

^eIFIMUP and IN - Institute of Nanoscience and Nanotechnology, and Department of Physics and Astronomy, Faculty of Sciences, University of Porto, 4169-007 Porto, Portugal

a very active hydrogenation catalyst and a hydrogen generator (from aqueous solution of NaBH₄) and this type of materials is attractive for the H₂ spillover mechanism.²⁹⁻³¹

Similarly, H₂ is the most promising energy fuel for automobiles 5 and small portable devices (eg. mobile phones and laptops) due to its light weight, high energy density and clean combustion. 13,32 Yet, significant challenges hinder its widespread application as a choice of fuel due to the lack of a safe and easy method of its storage. 33-35 Very recently, Li et al. reported the H2 storage 10 capacity of Pd crystal and Pd loaded HKUST at 303 K.36 However, specific synthesis protocol of porous material HKUST and overall dependency on precious metals was a major drawback. Therefore, it is crucial to develop new materials for efficient H2 storage as well. Considering the increasing need for $_{15}$ efficient H_2 storage (scheme 1) and the fact that Pd and Ni_xB are well-known materials for hydrogen spillover, we report a stepwise synthesis of Pd@NSG nanocomposite and systematic investigation of hydrogen spillover on Pd@NSG nanocomposite. For this, we have synthesized (i) RGO-SiO₂ nanocomposite then

(ii) Ni_xB-SiO₂/RGO and finally, (iii) Pd@Ni_xB-SiO₂/RGO 25 (Pd@NSG). Moreover, to synthesize the Ni_xB species on SiO₂/RGO nanocomposite, these steps are crucial due to high redox potential and hydrogen spillover capability of Pd compared to Ni, the entity Ni_rB can only form in the absence of Pd. Whereas, in one step synthesis there was chance of formation of 30 Pd-Ni alloy instead of Pd@Ni_xB entity. This is an economically viable method since it uses, as major components, low cost materials such as Ni_xB, SiO₂ and RGO and a small percentage of Pd as an activator. Moreover, in this work, the catalytic activity of Pd@NSG nanocomposite was investigated using the reduction 35 of 4-NP in an aqueous medium in the presence of NaBH₄. This is a standard hydrogenation reaction to evaluate the catalytic activity of nanocatalysts, owing to its ease of execution. ¹⁴ The H₂ spillover effect was confirmed through the high volumetric adsorption of the gaseous H2 in Pd@NSG nanocomposite and 40 also the disappearance of the phenolate absorbance peak at $\lambda \approx 400$ nm during the progress of 4-NP reduction to 4-AP.



Scheme 1 Schematic illustration of H₂ spillover on Pd and Ni_xB@ SiO₂ (left) and adsorption of H₂ in Pd@NSG nanocomposite (right).

Experimental Section

Materials

Flake graphite powder (particle size 100 mesh), palladium 70 acetate, nickel (II) acetate, 4-NP, KMnO₄, NaNO₃, H₂O₂ (30% v/v), NH₄OH, tetraethyl orthosilicate (TEOS, 98%), 3aminopropyl triethoxysilane (APTES, 99%), conc. H₂SO₄ (95-98%), conc. HCl (36.5-38%), methanol, ethanol and isopropanol (A.R. grades) and NaBH₄ were purchased from Sigma-Aldrich 75 Co. All other chemicals were of analytical grade and all aqueous solutions were prepared in Milli-Q water ($>18.2M\Omega.cm$).

Synthesis of GO

GO was synthesized by modified Hummer's method as described in previous work. 14 Briefly, flakes graphite powder (2.5 g) were 80 dispersed in conc. H₂SO₄ (90 mL) by magnetic stirring (45 min) at low temperature (0-5 °C). Later a calculated amount of NaNO₃ (1.25 g) and KMnO₄ (12.5 g) were added slowly and continuously stirred for 2 h. Next, temperature was raised to 35 °C for 1 h and 800 mL Milli-Q water was slowly poured in to the 85 acidic mixture. Furthermore, temperature was increased to 98 °C for 2 h. Finally, 35 mL of 30% v/v H₂O₂ was slowly poured to the reaction mixture to subside the further process. After completion of reaction, resultant suspension was centrifuged (3000 rpm) and washed (with Milli-Q water and dil. HCl) and 90 finally, freeze-dried and stored in a vacuum oven at RT.

Synthesis of SiO₂ /RGO nanocomposite

SiO₂ nanoparticles were synthesized by modified Stöber method. 16,37 Subsequently, 100 mL dispersion of GO was 5 prepared in methanol (1 mg/mL) by bath sonication (2 h). Later, for the preparation of RGO-SiO₂ nanocomposite, SiO₂ nanoparticles (1 g) were mixed in GO dispersion by repeated sonication and for GO reduction 50 mg NaBH₄ was added and mixed by magnetic stirring for 2 h at RT.

Synthesis of Ni_xB-SiO₂/RGO and Pd@NSG nanocomposite

To synthesize the Ni_xB-SiO₂/RGO nanocomposite, first nickel (II) acetate (240 mg) was dissolved in 5 mL DD water at RT and 15 mixed in above suspension. Subsequently, 20 mL alkaline aqueous solution of NaBH₄ (7 mg/mL, pH ~12.5) was slowly poured and mixed by mechanical stirring for 45 min at RT. After completion of reaction, resultant product was centrifuged (3000 rpm) and washed with Milli-Q water and ethanol. To synthesize Pd@NSG nanocomposite first, Ni_xB-SiO₂/RGO nanocomposite was dispersed in 100 ml anhydrous methanol by repeated sonication (30 min) at RT. Later, in above dispersion 10 mL palladium acetate solution (conc. 6 mg/mL in anhydrous methanol) was added and mixed by mechanically stirring for 2 h 25 at 45 °C. Finally, synthesized product was centrifuged at 3000 rpm and multiply washed with Milli-O water and methanol to remove the impurities and dried at 250 °C for 8 h.

Characterization

Phase purity and crystallinity were accessed by X-ray diffraction (XRD) technique (Rigaku, Japan, CuKα radiation: 2θ angle range 10-80°; step 0.02°/s). FTIR spectra of samples were recorded in ATR powder mode. Raman spectra were obtained at RT in back 35 scattering configuration with a Jobin-Yvon Lab Raman HR equipment. The XPS analysis was performed using a Kratos AXIS Ultra HSA, with VISION software for data acquisition and CASAXPS software for data analysis. The analysis was carried out with a monochromatic Al K_a X-ray source (1486.7 eV), 40 operating at 15kV (90 W), in FAT mode (Fixed Analyser Transmission), with a pass energy of 40 eV for regions ROI and 80 eV for survey. Data acquisition was performed with a pressure lower than 1.E-6 Pa, and it was used a charge neutralisation system. The effect of the electric charge was corrected by the 45 reference of the carbon peak (285 eV). The deconvolution of spectra was carried out using the XPSPEAK41, in which a peak fitting is performed using Gaussian-Lorentzian peak shape and Shirley type background subtraction. Surface morphology of GO and products were investigated by scanning electron microscope 50 (SEM) SU-70 Hitachi in EDX mode. For TEM analysis conventional high-resolution (HR) TEM technique was used. The sample for TEM was prepared by dipping an aliquot of suspension (in methanol, 0.1 mg/mL) on to a carbon-coated copper grid and dried at RT. Volumetric H₂ storage 55 measurements were carried out at 298 K using Sievert's instrument. Approximate, 1 g samples were used for adsorption isotherm and prior to measurements, samples were out gassed at 250 °C for 12 h. Each time, the calibration and void volume calculation were carried out at RT under high purity helium 60 atmosphere. UV-vis spectra were collected by Shimadzu UV-2501PC (UV-vis) spectrophotometer in the absorbance mode.

Catalytic reduction of 4-NP

65 The nanocomposite catalytic tests were performed as follows: 1 mL of each reactant aqueous solution, 4-NP (0.1 mM) and NaBH₄ (0.3 M) was transferred to a quartz cuvette and the mixture was sonicated for 2 min. Followed by, 5 mg of the catalyst was added in order to start the reaction. The intensity of 70 the absorption peak at $\lambda = 400$ nm was used to monitor the process of the conversion of 4-NP to 4-AP.

Results and discussion

Fig. 1 (a) shows the XRD of GO, Ni_xB-SiO₂/RGO and Pd@NSG nanocomposite. GO exhibits a sharp peak at around 11.2° which 75 corresponds to the (001) basal plane suggesting the good exfoliation of graphite flakes due to the larger value of d-spacing (0.79 nm) of GO compared to 0.334 nm of graphite (2 θ =26.4°).^{38'} It is well-known that after a vigorous oxidation of graphitic flakes in strong oxidizing environment, different kinds 80 of oxygenated functional groups are attached to the graphitic plane and increase the interlayer spacing of graphitic sheets. 14 In XRD spectra of Ni_xB-SiO₂/RGO nanocomposite, the peak related to GO was completely suppressed and a new peak is observed at 22.8°, which suggests the successful reduction process and 85 formation of reduced graphene oxide (RGO).

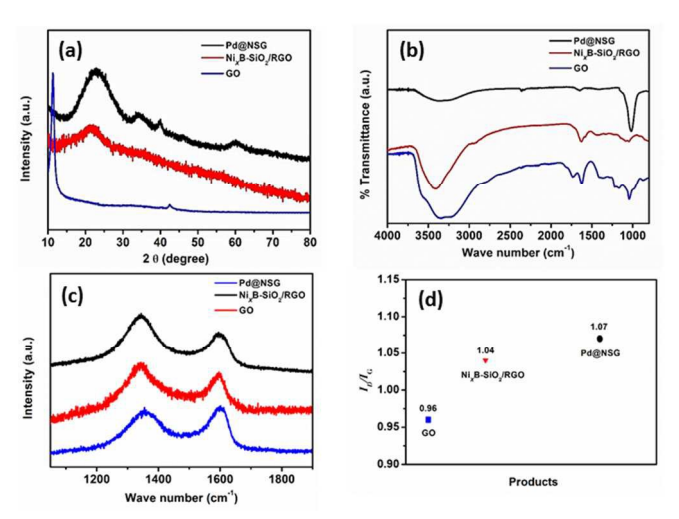
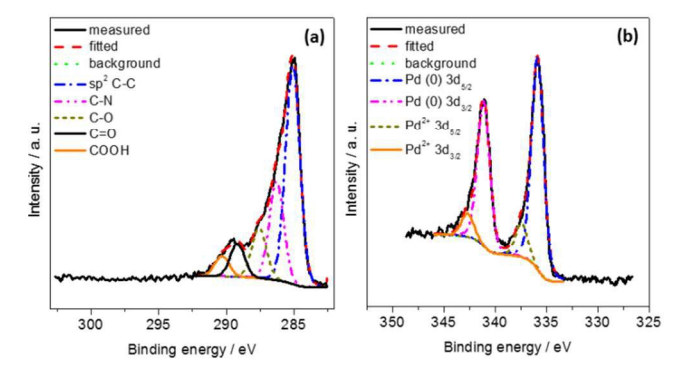


Fig.1 Spectroscopic analysis of GO, Ni_xB-SiO2/RGO and Pd@NSG nanocomposite: (a) XRD pattern, (b) FTIR and (c) Raman spectroscopy; and (d) 90 Interpretation of Raman spectroscopy with accordance of I_D/I_G ratio of GO, Ni_xB-SiO2/RGO and Pd@NSG nanocomposite.

The XRD spectra of Pd@NSG shows some additional peaks that are also related to the various crystallographic diffraction planes of Pd/PdO phase. The major diffraction peaks at 39.9° and 46.4° 95 can be assigned as diffraction from (111) and (200), respectively, planes of face-centered cubic (fcc) crystal lattice structure of Pd.³⁹ The other two peaks at 34.29° and 59.9° indicates the reflection from PdO (due to surface oxidation of Pd).⁴⁰ In addition, in order to elucidate the structure of Pd@NSG 100 nanocomposite and reaction mechanism in more detail, we have also carried out the FTIR spectroscopy. Fig. 1(b) shows the FTIR spectra of GO, Ni_xB-SiO₂/RGO and Pd@NSG nanocomposite (in the range of 4000-800 cm⁻¹). In FTIR spectra of GO, a strong broad band was observed in the high frequency area (3400-3200 105 cm⁻¹) which is assigned to the vibration stretching mode of -OH groups due to the surface adsorbed water molecules. After the reduction, the intensity of this band was continuously decreased

from Ni_xB-SiO₂/RGO to Pd@NSG nanocomposites which suggests the subsequent removal of surface adsorbed water molecules during the reduction process.⁴¹ Moreover, the peak related to the vibration stretching mode of carbonyl functionality 5 also became deprived in Ni_xB-SiO₂/RGO to Pd@NSG nanocomposites indicating the elimination of edge related -C=O groups and formation of GO to RGO.¹⁴ Finally, the absorption peaks at 1385 cm⁻¹ (stretching vibration of C-O of carboxylic acid) and 1110 cm⁻¹ (C-OH of alcohol) were also efficiently 10 reduced in both samples compared to the GO.41 However, in Ni_xB-SiO₂/RGO and Pd@NSG nanocomposites a new peak was observed at 1008 cm⁻¹ which indicates the incorporation of SiO₂ nanoparticles. 42 Then, to ascertain the change in carbon system Raman spectroscopy was also performed. This technique is very 15 useful for assigning the corresponding changes of graphene material on the basis of peak position and intensity. Fig. 1 (c) shows the Raman spectra of GO. Ni_vB-SiO₂/RGO and Pd@NSG nanocomposite in the range of 1050-1900 cm⁻¹. The Raman spectrum of GO displays the two characteristic D and G bands at ²⁰ 1353 and 1598 cm⁻¹, respectively, with an I_D/I_G ratio of 0.96. It has already been reported that the G band is an intrinsic feature of graphene and closely related to the vibrations in all sp² carbon materials.¹⁴ The D band becomes prominent when defects are introduced in graphene and in GO it is activated due to the 25 reduction in size of the in-plane sp² domains due to the attachment of various functionalities in edge and basal plane sites. 41 In Ni_xB-SiO₂/RGO and Pd@NSG nanocomposite spectra, these two prominent bands (D and G) were shifted to lower wave numbers and are located at 1346 and 1596 and 1343 and 1594 30 cm⁻¹, respectively. In both spectra I_D/I_G ratio was increased compared to GO. The continuous increment of I_D/I_G ratio from GO to Ni_xB-SiO₂/RGO and Pd@NSG nanocomposite can be clearly observed in Fig. 1(d) suggested the clear change in carbon system due to the incorporation of some extra defects in 35 graphene.3

We have also performed the XPS analysis to identify the degree of reduction from GO to RGO and investigated the oxidation states of Pd, Ni, B and Si entities in Pd@NSG nanocomposite. The C 1s XPS spectrum of GO shows two large 40 broad peaks that are deconvoluted into four peaks at approximately 284.3, 285.2, 287.2 and 288.9 eV (see Fig. S1 supplementary information). The peaks at 284.3 and 285.2 eV are attributed to the sp² C=C and sp³ C-C bonding, respectively.¹⁴ The peak at around 287.2 eV is assigned to the binding energies 45 of carbon in C-O and C=O and that at 288.9 eV to carbon in COOH groups. 43



50 Fig. 2 Deconvoluted XPS spectra for Pd@NSG: (a) C 1s and (b) Pd 3d.

However, the C 1s core level spectrum of Pd@NSG (Fig. 2a) shows one intense peak and another less intense at higher binding energies. These peaks are deconvoluted into five peaks at

approximately 285.0, 286.3, 287.6, 289.2 and 290.3 eV. The peak 55 at 285.0 is attributed to sp² C-C, ⁴⁴ that at 286.3 eV to C-N, the ones at 287.6 and 289.2 eV to binding energies of carbon in C-O (hydroxyl and epoxy) and C=O, respectively. Similarly the peak at around 290.3 eV corresponds to carbon in COOH groups. 43, 45-⁴⁶ Normally, the peak intensity due to C-O and C=O is very high 60 in GO. But our results show the less intense peak, which is proportionate to the reduction of GO to RGO during the metal NPs (Ni and Pd) deposition. 43, 47 During this process there was an easy spillover of hydrogen gas on metal NPs which further reduces the oxygen functionalities of GO. The deconvoluted 65 spectra of O 1s, B 1s, N 1s, Si 2p and Ni 2p are shown in Figure S2 (see supplementary information). In Table S1 (see supplementary information) are summarized the XPS data obtained for Pd@NSG. The XPS spectrum of Pd 3d is shown in Fig 2b. The binding energies of Pd 3d can be resolved into $3d_{5/2}$ 70 and 3d_{3/2} doublets caused by spin-orbital coupling. Upon deconvolution of the spectra, the curves are fitted with two pairs of binding energies for Pd⁰ and Pd^{II} at 335.8eV, 341.1 eV and 337.4eV, 342.7 eV, respectively.⁴⁸ The percentage of Pd^{II} relatively to Pd⁰ is 12.5%. The O 1s core level spectrum of 75 Pd@NSG (Fig. S2a, supplementary information) is deconvoluted into 2 main peaks approximately at 531.8 and 533.5 eV assigned to O=C-OH and O-C or C-OH, respectively. 46, 49 The Ni 2p spectrum is also deconvoluted into $2p_{3/2}$ and $2p_{1/2}$ doublets caused by spin-orbital coupling. The peak of metallic nickel is observed 80 at approximately 853.5 eV, while those at 857.0 and 874.4 eV and 862.2 and 880.6 eV are attributed to NiO and NiOOH, respectively (see Fig. S2e, supplementary information). 50,51

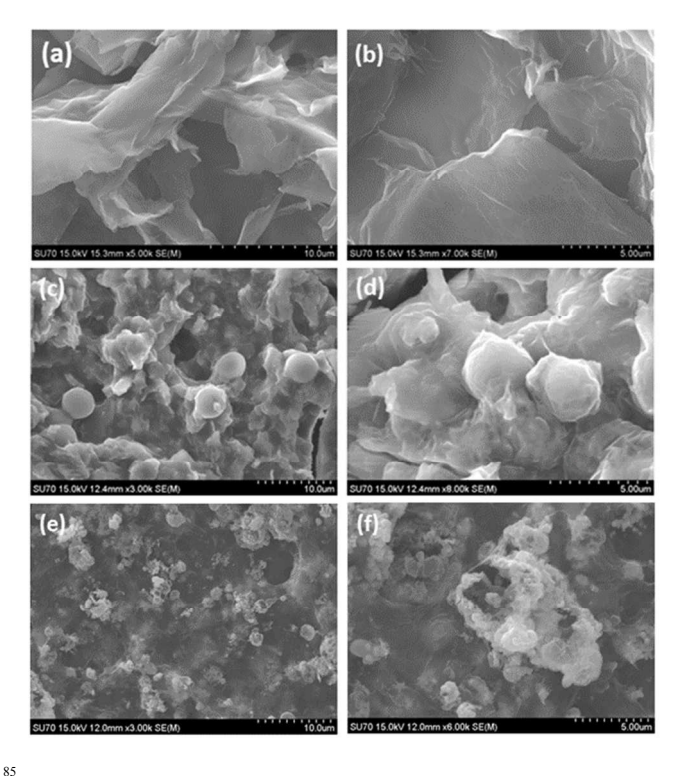
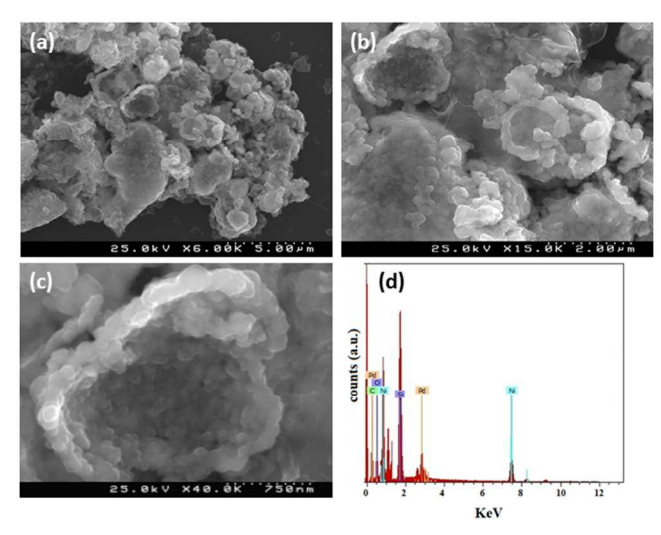


Fig.3 SEM images of: GO (a) and (b), SiO₂/RGO (c) and (d) and Ni_xB-SiO₂/ RGO nanocomposites (e) and (f) in higher and lower magnifications, respectively.

90 The existence of B species is confirmed by the presence of sharp peak at 193 eV in B 1s XPS core spectrum. 52-53 Systematic microscopic investigations of initial material GO, intermediate

composite material RGO-SiO₂ (after the loading of synthesized SiO₂ nanoparticles within the RGO matrix), Ni_xB-SiO₂/RGO nanocomposite and final product Pd@NSG nanocomposite were also carried out. Fig. 3 (a) and (b) show the SEM images of GO 5 (after the 2 h exfoliation in methanol at RT) at higher and lower magnifications, respectively. Images of GO clearly exhibit the presence of few layers of graphitic carbon with typical wrinkle behaviour.³⁸ Fig. 3 (c) and (d) display the initial morphology and size of the SiO₂ nanoparticles with graphene sheet and show that 10 all particles were small sized and with spherical shape. Moreover, images shows that SiO₂ nanoparticles are covered with carbon sheets and well separated without any specific agglomerations.⁵⁴ Similar behaviour was observed after the intercalation of Ni_xB nanoparticles on SiO₂/RGO as observed in Figs. 3 (e) and (f). 15 Additionally, these two images show higher density of nanoparticles compared to previous images of SiO₂/RGO indicating the successful formation of Ni_xB-SiO₂/RGO nanocomposite. Fig.4 (a-c) shows the SEM images of the final product Pd@NSG at different magnifications. Fig. 4 (a) and (b), 20 at lower magnification, show the intercalation of tiny Pd nanoparticles on Ni_xB-SiO₂/RGO nanocomposite at a superficial position and Fig. 4 (c) depicts the arrangement of the nanoparticles in a cone-type structure. This arrangement may be due to the grafting of small Pd nanoparticles on high defect sites 25 of Ni_xB-SiO₂/RGO nanocomposite and the filling of cavities by them. Moreover, to confirm the presence of Ni and Pd elements, we also have carried out the EDX analysis.



 $_{\rm 30}\,$ Fig.4 SEM images of Pd@NSG nanocomposite at different magnifications: 6000x (a) 15000x (b) and 40000x (c); (d) EDX spectra of Pd@NSG.

Fig. 4 (d) displays the EDX spectrum of Pd@NSG nanocomposite and results show the presence of all elements: Pd, Ni, Si, C and O with the exception of the light weight elements B 35 and H. TEM analysis was also performed to confirm the shape, morphology and internal structure of Pd@NSG nanocomposite for detailed investigation of final product. Fig. 5 (a) and (b) show the TEM images at lower and higher magnification, respectively. The images clearly displays the homogeneous distribution of 40 nanoparticles on the graphene sheets; the higher magnification image shows that all particles have spherical shape without any specific kind of agglomeration of nanoparticles. 55 Moreover, to find the crystallinity in Pd@NSG nanocomposite we have performed the selected area electron diffraction (SAED) analysis 45 (see Fig. S3 supplementary information) which clearly shows the (111) lattice fringe of Pd NPs along with bright spots of graphene layers.⁵⁵ Furthermore, to establish the detailed mechanism of

reduction of Pd2+ ions to Pd (0) in presence of anhydrous methanol (CH₃OH), ⁵⁶ we have also carried out the HRTEM 50 analysis of bare Pd NPs which clearly shows the formation of monodisperse small spherical Pd NPs in the range of (2.5-4 nm) without any agglomeration (see Fig. S4 supplementary information for detail). Here, we used Pd(OAc)₂ precursor and as solvent and reducing agent. At moderate 55 temperature (45°C) and under sonication condition methanol provided the reducing species H₂ as per the following equation

$$2 \text{ CH}_3\text{OH} = 2 \text{ HCHO} + \text{H}_2.....$$
 (1)

Also, the produced H₂ reduces the Pd (OAc)₂ to Pd(0) as shown in equation (2).

$$Pd(OAc)_2 + H_2 = Pd(0) + 2CH_3COOH....(2)$$

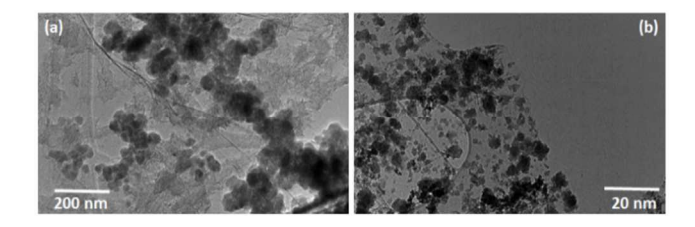


Fig.5. TEM images (a) and (b) of Pd@NSG nanocomposite at higher and 70 lower magnifications, respectively.

Finally, to investigate the spillover effect we have performed the physical H₂ storage measurement using Sievert's instrument and isotherms were recorded under pressure from 1-50 bar. Fig. 6 shows the H₂ uptake characteristic of SiO₂/RGO, Ni_xB-75 SiO₂/RGO, Pd-SiO₂/RGO and Pd@ NSG nanocomposite at RT. As displayed in the graph, the H₂ storage increases in the materials with increasing pressure.

At 50 bar, the maximum H₂ storage of SiO₂/RGO is 0.25 mmol while, after insertion of nanoparticles in SiO₂/RGO matrix the H₂ 80 uptake capacity was dramatically increased. For Ni_xB-SiO₂/RGO and Pd-SiO₂/RGO nanocomposites the maximum H₂ uptake was estimated to be 0.76 and 1.55 mmol, respectively. At similar adsorption isotherm conditions the major changes were obtained for Pd@NSG nanocomposite which shows a 3.5 mmol H₂ uptake. 85 This value was approximately 14 times higher than SiO₂/RGO

nanocomposite. The corresponding wt. % values were 0.05 and 0.7, respectively. This shows the enhancement of H₂ uptake in Pd@NSG sample which was higher than SiO₂/RGO in the whole range of pressures tested.

Scheme 1 illustrates the H₂ spillover mechanism and subsequent diffusion in Pd@NSG nanocomposite. Here, the metal nanoparticles (Pd and Ni_xB@SiO₂) act as spillover centre for H₂ molecules and dissociates the molecular H₂ into H radicals.⁵⁶ The generated H radicals then migrates from the 95 catalyst centre to the storage material and easily diffuse into the graphene layers.⁵⁷ Especially, they migrate to the defect sites of graphene sheets such as the edges locations and saturate the hexagonal sp² hybridized (-C=C) network and make the sp³ hybridized (-C-H) structure. 38 This phenomenon can be explained 100 through the formation of "bridge" built structure on catalyst centre where H₂ molecules easily form the dangling bonds with catalyst centre and dissociate into H^{*} radicals.³⁰ In detail, the Pd nanoparticles work as a source, the Ni_xB nanoparticles act as an

activator to dissociate the H2 molecules and finally, RGO and SiO₂ play the role of receptor.

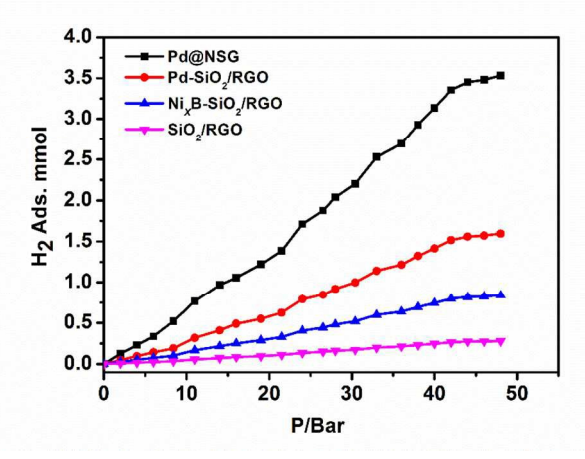


Fig.6 H₂ adsorption isotherm of SiO₂/RGO, Ni_xB-SiO₂/RGO, Pd-SiO₂/RGO 5 and Pd@NSG nanocomposite up to 50 bar pressure at RT

Due to this process an adduct species on catalyst surface is formed by the dissociation of H_2 molecule and subsequently, π - π bonding (-C=C) of graphene gets saturated and form sp³ (C-H) bonding.³⁸ Finally, RGO works as a primary receptor site for 10 preferential storage of H radicals via chemisorption and SiO2 nanoparticles act as a secondary receptor to adsorbs the H2 molecule by physisorption.³⁰ Due to these facts, the obtained result of H₂ uptake for Pd@NSG nanocomposite at RT was remarkably higher than previously reported works. 35,58 Huang *et* 15 al. reported 0.15 wt. % of H₂ storage in Pd-Gr nanocomposite at similar conditions (298 K and 60 bar).⁵⁹ Although, they have noticed that after loading of Pd metal on the graphene sheet, the H₂ uptake was doubled. It is obviously due to the spillover capability of Pd to dissociate the H₂ molecules and subsequent 20 migration of H atoms on graphene sheet. The results reported here are also better than those obtained by Anson et al. 60 They reported a 0.16 wt. % H₂ storage at RT in Pd nanoparticles intercalated single walled carbon nanotube (SWNT) after applying 90 bar. However, in our work we applied only a 25 maximum pressure of 50 bar and a 4 times higher H₂ storage was observed. This may be attributed due to the porous structure of SiO₂, edge defects and large surface area of graphene along with the presence of two spillover centres. Our results of storage capacity of Pd@NSG are higher compared to Latroche et al. 61 in 30 the giant-pore MOF MIL-101 (~0.43 wt. % at 80 bar), and Campesi et al.62 in Pd nanoparticles loaded porous carbon template composites at 298 K (0.08 wt. % H₂ storage).

The reduction of 4-NP by NaBH₄ is a standard reaction in which the presence of the catalyst is the essential part for final 35 accomplishment of the reaction. This reaction can be easily monitored by UV-vis spectroscopy under ambient conditions. In absence of the catalyst, NaBH4 only produces the 4nitrophenolate intermediate ion (peak at 400 nm) in aqueous medium due to the increment of neutral aqueous solution 40 alkalinity which is maintained for several hours (Fig. 7(a)). After the addition of Pd@NSG catalyst, the peak related to 4-NP was drastically decreased and almost disappeared within 2 min (120 s) as depicted in Fig. 7(b). At the same time, a new peak appears at around 300 nm which suggests the successful reduction process 45 and the formation of 4-AP confirming the high catalytic activity of Pd@NSG nanocomposite compared to previously reported works. 63,64 This higher catalytic activity of Pd@NSG nanocomposite can be attributed to the presence of bi-metallic

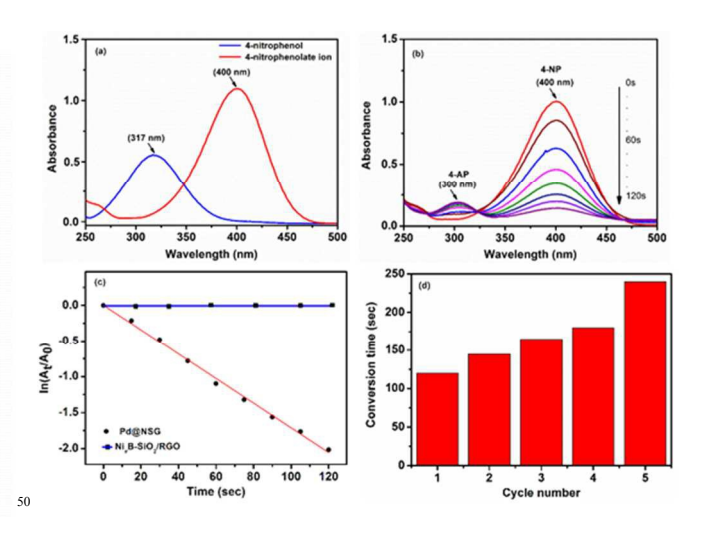
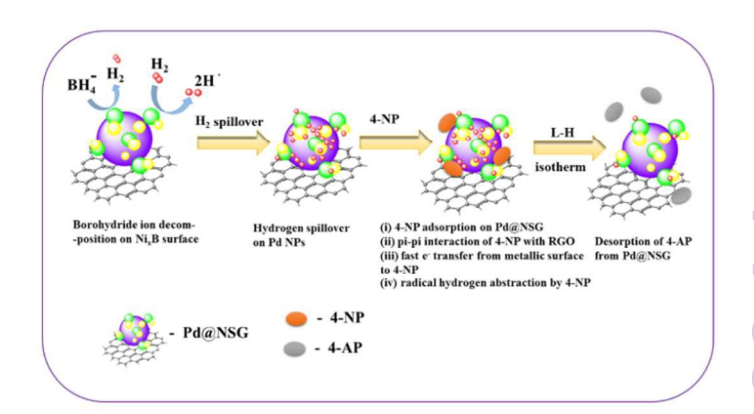


Fig.7 UV-vis spectra of (a) 4-NP molecule initially and after the addition of NaBH₄ in aqueous medium at 25 °C and (b) time dependent reduction process after the addition of Pd@NSG nanocatalyst in reaction medium. 55 (c) Pseudo-first order plots of 4-NP reduction catalysed by Pd@NSG (red) and NixB-SiO₂/RGO (blue) in the presence of NaBH₄. (d) Stability measurement of Pd@NSG nanocatalyst during 5 successive cycles.

condition of two well-known hydrogenation reaction catalyst (Pd and Ni_xB). In this aspect we also investigated the role of 60 individual components viz. SiO₂/RGO matrix, Ni_xB-SiO₂/RGO, Pd-SiO₂/RGO without altering reaction conditions and protocol. SiO₂/RGO matrix shows the negligible extent of reduction whereas, Ni_xB-SiO₂/RGO and Pd-SiO₂/RGO reduces the 4-NP, but the rate of reaction was too slow compared to Pd@NSG 65 nanocomposite and estimated times were 22 (1320 s) and 120 min (7200 s), respectively (see Fig. S5 supplementary information).



Scheme 2 Schematic representation of 4-NP molecule reduction on Pd@NSG nanocomposite in presence of NaBH₄ in aqueous medium.

Further, we have performed the kinetic measurement of 75 Pd@NSG nanocomposite as shown in Fig. 7(c). The kinetics of the catalytic reaction measured as a function of time on the basis of absorbance at 400 nm.16 In this reaction, the concentration of NaBH₄ was in excess compared with 4-NP and can be regarded as constant throughout the reaction and pseudo-first-order kinetics 80 can be applied with respect to 4-NP.²¹ A linear relationship was obtained between $ln(A_t/A_0)$ and reaction time (t) which directly inferred the concentration of 4-AP during the reaction as $ln(C_1/C_0)$ as given in equation 3.

$$5 k = t^{-1} \ln(C_t/C_0) = t^{-1} \ln(A_t/A_0)$$
 (3)

where k is the apparent rate constant, and A_t and A_0 are the concentrations of 4-NP at time t and 0, respectively. 16 The calculated value of k was 0.017 s^{-1} for Pd@NSG nanocomposite, 10 a value higher than previously reported works. 16,19,21 From Fig. 7 (c) it is clearly indicated that lnA400 shows a good linear correlation and a R² of 99.97. This linear relationship for Pd@NSG catalysts, indicate that the reaction follows first-order kinetics. The rate constants for different catalysts were also 15 estimated from diffusion-coupled first order reaction kinetics using the slopes of the straight lines and are given in (see Fig. S6) supplementary information). The rate constant for Pd-SiO₂/RGO was about twelve times lower than that obtained for Pd@NSG nanocomposites showing the catalytic activity of Pd nanoparticles 20 remarkably improved by combining only with the Ni_xB entity. The rate constant of Ni_xB-SiO₂/RGO was too low compared with Pd based nanocomposite, imposing slow kinetic behaviour (see supplementary information for detail). Moreover, in this context, a second constant K ($K = k \text{ (min}^{-1})/ n_{Pd} \text{ (mmol)}$) was also 25 determined, 16 normalizing the k value to the Pd surface contents determined by XPS (0.8 Atomic %) which is equal to 0.75 mmol/gm. The calculated K value was $4.53 \text{ mmol}^{-1} \text{ s}^{-1}$ or 272 mmol^{-1} mmol^{-Γ} min⁻¹, indicating high catalytic performance of Pd@NSG compared to previously reported work.⁶

Finally, we have performed the recycling test of Pd@NSG nanocomposite also for reduction of 4-NP organic molecule by the insertion of additional aliquots (25 µl) of reagents in same reaction cell. After each addition, the UV was recorded and the catalysts exhibited well stability towards the 4-NP reduction and 35 corresponding time was increased up to 240 s for 5th cycle as shown in Fig. 7(d), suggests the robustness of catalyst at least for 5 consecutive cycles with an efficiency of 88 %.

Conclusions

In this work, we have successfully synthesized Pd@NSG 40 nanocomposite and characterised by various techniques. The successful reduction of GO was analysed by XRD, FTIR and Raman techniques which exhibits the change in carbon structure. Moreover, the formation of Pd nanoparticles was also studied using the XRD technique. To investigate the presence of Ni 45 element in nanocomposite (due to formation of amorphous phase Ni_xB) EDX analysis was carried out. H₂ uptake measurements of up to 50 bar pressure clearly exhibited 14 times more storage at RT in Pd@NSG nanocomposite compared to SiO₂/RGO. Such a high storage of H₂ is attributed to the spillover mechanism on Pd 50 and Ni_xB on graphene sheet which can make the avenue for new developments in future H2 economy. Moreover, Pd@NSG displayed the ultrafast response for reduction of environmental pollutant 4-NP with remarkable high stability and catalytic activity. This feature suggested the extra benefit of product for 55 catalysis of nitro organic compound reduction.

Acknowledgements

The authors gratefully acknowledge FCT Portugal. R.K. and E.T. 60 thankful to FCT for grant (PTDC/EME-MFE/103051) and (SFRH/BD/80105/2011) for their financial support. D. F. thanks FCT for her post doc fellowship SFRH/BPD/74877/2010. J. V. acknowledges financial support through FSE/POPH. C. D. is

thankful to FCT for grant SFRH/BI/52521/2014. The authors 65 acknowledge funding from FEDER and ON2 through project Norte-070124-FEDER-000070.

Notes and references

- S. Yang, J. Dong, Z. Yao, C. Shen, X. Shi, Y. Tian, S. Lin and X. Zhang, Sci. Rep., 2014, 4, 4501.
- S. Kumar, C. Selvaraj, L. G. Scanlon and N. Munichandraiah, Phys. Chem. Chem. Phys., 2014, 16, 22830-22840.
- J. Liu, H. Zhou, Q. Wang, F. Zeng and Y. Kuang, J. Mater. Sci., 2012. 47. 2188-2194.
- L. Shao, X. Huang, D. Teschner and W. Zhang, ACS Catal., 2014, 4, 2369-2373.
- R. Nie, J. Wang, L. Wang, Y. Qin, P. Chen and Z. Hou, Carbon N. *Y.*, 2012, **50**, 586–596.
- L. Castro, M. L. Blázquez, J. Á. Muñoz, F. G. González and A. Ballester, Rev. Adv. Sci. Eng., 2014, 3, 199-216.
- S. Wei, Q. Wang, J. Zhu, L. Sun, H. Lin and Z. Guo, Nanoscale, 2011, 3, 4474.
- D. Chen, X. Zhao, S. Chen, H. Li, X. Fu, Q. Wu, S. Li, Y. Li, B. L. Su and R. S. Ruoff, Carbon N. Y., 2014, 68, 755-762.
- Y. Wang, Y. Zhao, J. Yin, M. Liu, Q. Dong and Y. Su, Int. J. Hydrogen Energy, 2014, 39, 1325-1335.
- 10 R. Krishna, E. Titus, L. C. Costa, J. C. J. M. D. S. Menezes, M. R. P. Correia, S. Pinto, J. Ventura, J. P. Araújo, J. A. S. Cavaleiro and J. J. A.Gracio. J. Mater. Chem., 2012, 22, 10457-10459.
- N. Atar, T. Eren, M. L. Yola, H. Karimi-Maleh and B. Demirdögen, RSC Adv., 2015, 5, 26402-26409.
- 12 S. Wu, Q. He, C. Zhou, X. Qi, X. Huang, Z. Yin, Y. Yang and H. Zhang, Nanoscale, 2012, 4, 2478.
- Y. Qin, J. Wang, F. Meng, L. Wang and X. Zhang, Chem. Commun. (Camb)., 2013, 49, 10028-30.
- R. Krishna, D. M. Fernandes, C. Dias, J. Ventura, E. Venkata Ramana, C. Freire and E. Titus, Int. J. Hydrogen Energy, 2015, 40,
- 100 15 Z. D. Pozun, S. E. Rodenbusch, E. Keller, K. Tran, W. Tang, K. J. Stevenson and G. Henkelman, J. Phys. Chem. C, 2013, 117, 7598-
 - 16 M. Rocha, C. Fernandes, C. Pereira, S. L. H. Rebelo, M. F. R. Pereira and C. Freire, RSC Adv., 2015, 5, 5131-5141.
- M. Ayán-Varela, M. J. Fernández-Merino, J. I. Paredes, S. Villar-Rodil, C. Fernández-Sánchez, L. Guardia, a. Martínez-Alonso and J. M. D. Tascón, J. Mater. Chem. A, 2014, 2, 7295.
- 18 B. K. Barman and K. K. Nanda, Appl. Catal. A Gen., 2015, 491, 45-51.
- 110 19 R. Ren, S. Li, J. Li, J. Ma, H. Liu and J. Ma, Catal. Sci. Technol.,
 - W. Sun, X. Lu, Y. Tong, Z. Zhang, J. Lei, G. Nie and C. Wang, Int. J. Hydrogen Energy, 2014, 39, 9080-9086.
- Z. Ji, X. Shen, G. Zhu, H. Zhou and A. Yuan, J. Mater. Chem., 2012, **22**, 3471.
- 22 P. Á. Szilágyi, E. Callini, a Anastasopol, C. Kwakernaak, S. Sachdeva, R. van de Krol, H. Geerlings, a Borgschulte, a Züttel and B. Dam, Phys. Chem. Chem. Phys., 2014, 16, 5803-9.
- 23 K. Bhowmik, D. Sengupta, B. Basu and G. De, RSC Advances, 2014, 4, 35442-35448.
- 24 Y. Hou and S. Gao, J. Mater. Chem., 2003, 13, 1510–1512.
- 25 R. Eluri and B. Paul, J. Nanoparticle Res., 2012, 14, 1-14.
- 26 N. Cordente, M. Respaud and F. Senocq, Nano Lett., 2001, 2, 2-5.
- 27 D. de Caro and J. S. Bradley, *Langmuir*, 1997, **13**, 3067–3069.
- 125 28 H. I. Schlesinger, H. C. Brown, A. E. Finholt, J. R. Gilbreath, H. R. Hoekstra and E. K. Hyde. J. Am. Chem. Soc., 1953, 75, 215-219.
 - Y. Chen and H. Kim. Fuel Process Technol., 2008, 89, 966-972.
- 30 R. Krishna, E.Titus, M. Salimian, O. Okhay, S. Rajendran, A. Rajkumar, J. M. G. Sousa, A. L. C. Ferreira, J. C. Gil and J. Gracio, Hydrogen Storage for energy application, Intech Open, Europe 2012,
- A. J. Lachawiec, G. Qi and R. T. Yang. Langmuir, 2005, 21, 11418-11424.

- S. J. Peighambardoust, S. Rowshanzamir and M. Amjadi. Int. J. Hydrogen Energy, 2010, 35, 9349–9384.
- 33 H. Kobayashi, H. Morita, M. Yamauchi, R. Ikeda, H. Kitagawa, Y. Kubota, K. Kato and M. Takata, J. Am. Chem. Soc., 2011, 133, 11034-11037.
- 34 G.K. Dimitrakakis, E. Tylianakis and G. E. Froudakis. Nano Lett., 2008, 8, 3166-3170.
- 35 G. Srinivas, Y. Zhu, R. Piner, N. Skipper, M. Ellerby and R. S. Ruoff, *Carbon*, 2010, 48, 630-635.
- 10 36 G. Li et al. Nat. Mater., 2014, 13, 802-806.
 - 37 I. A. M. Ibrahim, A. A. F. Zikry and M. A. Sharaf, J. Am. Sci., 2010, 6, 985–989.
 - 38 R. Krishna, E. Titus, O. Okhay, J. C. Gil, J. Ventura, E. Venkata Ramana, J. J. A. Gracio. Int. J. Electrochem. Sci., 2014, 9, 4054-4069.
 - 39 B. K. Barman and K. K. Nanda, Appl. Catal. A Gen., 2015, 491, 45-51
 - 40 C. J. Huang, F. M. Pan, T. C. Tzeng, L. Chang and J.T. Sheu. J. Electrochem. Soc., 2009, 156, J28-31.
- 20 41 X. Mei and J. Ouyang, Carbon, 2011, 49, 5389-5397.
 - 42 H. R. N. and N. S. and M. R. R.-A. and M. M. B. M. and E. K. Goharshadi, *Phys. Scr.*, 2013, **87**, 025802.
 - 43 D. R. Dreyer, S. Park, C. W. Bielawski and R. S. Ruoff, *Chem. Soc Rev.*, 2010, 39, 228-240.
- 25 44 L. Chen, Z. Xu, J. Li, B. Zhou, M. Shan, Y. Li, L. Liu, B. Li and J. Niu, RSC Adv., 2014,4, 1025-1031.
 - 45 Z. Lin, Y. Yao, Z. Li, Y. Liu, Z. Li and C.-P. Wong, J. Phys. Chem. C, 2010, 114, 14819–14825.
- 46 S. Park, J. An, J.R. Potts, A. Velamakanni, S. Murali, R.S. Ruoff, *Carbon*, 2011, **49**, 3019–3023.
- 47 A. Ganguly, S. Sharma, P. Papakonstantinou and J. Hamilton, J. Phys. Chem. C, 2011, 115, 17009–17019.
- 48 M. Górna, M. S. Szulmanowicz, A. Gniewek, W. Tylus and A. M. Trzeciak, J. Organometallic Chem. 2015, 785, 92-99.
- 35 49 Y. J. Oh, J. J. Yoo, Y. II Kim, J. K. Yoon, H. N. Yoon, J.-H. Kim, S. B. Park, Electrochemica Acta, 2014, 116, 118-128.
 - 50 Y. Zhao, X. Yang, J. Tian, F. Wang, L. Zhan, Int. J. Hydrogen Energy, 2010, 35, 3249-3257.
- 51 K. Bhowmik, A. Mukherjee, M. K. Mishra and G. De, *Langmuir*, 2014, **30**, 3209-3216.
- 52 J. A. Schreifels, P. C. Maybury and W. E. Swartz, J. of Catalysis, 1980, 65, 195-206.
- 53 J. Legrand, A. Taleb, S. Gota, M.-J. Guittet and C. Petit, *Langmuir* 2002, 18, 4131-4137.
- 45 54 W. L. Zhang and H. J. Coi, Langmuir, 2012, 28, 7055-7062.
 - 55 T. Sun, Z. Zhang, J. Xiao, C. Chen, F. Xiao, S. Wang and Y. Liu, Sci. Rep., 2013, 3, 2527.
 - 56 P.D. Burton, T. J. Boyle, A. K. Datye, J. of Catalysis, 2011, 280, 145-149.
- 50 57 Y. She, Z. Lu, W. Fan, S. Jewell and M. K. H. Leung, J. Mater. Chem. A, 2014, 2, 3894.
 - 58 L. Wang, J.A.J. Lachawiec and R.T. Yang. RSC Adv., 2013, 3, 23935-23952.
- C. C. Huang, N. W. Pu, C. A. Wang, J. C. Huang, Y. Sung, M. D.
 Ger. Separ. Purif. Tech., 2011, 82, 210–215.
- 60 A. Ansón, M. a. Callejas, a. M. Benito, W. K. Maser, M. T. Izquierdo, B. Rubio, J. Jagiello, M. Thommes, J. B. Parra and M. T. Martínez. *Carbon*, 2004, 42, 1243-1248
- 61 M. Latroche, S. Surblé, C. Serre, C. Mellot-Draznieks, P. L. Llewellyn, J. H. Lee, J. S. Chang, H. J. Sung and G. Férey, *Angew. Chemie Int. Ed.*, 2006, 45, 8227–8231.
- 62 R. Campesi, F. Cuevas, R. Gadiou, E. Leroy, M. Hirscher, C. Vix-Guterl, M. Latroche. *Carbon*, 2008, 46, 206-214.
- 63 H. Li, L. Han, J. C. White and I. Kim, *Green Chem.*, 2012, **14**, 586-591.
- 64 S. Zhang, S. Gai, F. He, S. Ding, L. Li and P. Yang, *Nanoscale*, 2014, 6, 11181–11188.
- 65 M. Zhu, B. Lei, F. Ren, P. Chen, Y. Shen, B. Guan, Y. Du, T. Li and M. Liu, Sci. Rep., 2014, 4, 5259.